8-1-2022

An innovative algorithm based on wavelets for solving three-dimensional nanofluid bio-convection model near a stagnation point

Mutaz Mohammad
Zayed University

Alexander Trounev
Kuban State Agrarian University

Mohammed Alshbool
Zayed University

En-Bing Lin
Wentworth Institute of Technology

Results in Physics 41 (2022) 105889

Contents lists available at ScienceDirect

Results in Physics

journal homepage: www.elsevier.com/locate/rinp

An innovative algorithm based on wavelets for solving three-dimensional nanofluid bio-convection model near a stagnation point

Mutaz Mohammad [a,*], Alexander Trounev [b], Mohammed Alshbool [a], En-Bing Lin [c]

[a] Zayed University, United Arab Emirates
[b] Kuban State Agrarian University, Russia
[c] Wentworth Institute of Technology, United States of America

ARTICLE INFO

Keywords:
Stagnation point
Euler wavelets
Collocation points
Numerical approximation
Nanofluid
Nonlinear ordinary differential equations

ABSTRACT

In this article, we are mainly targeting a new numerical algorithm based on Euler wavelets for solving a system of partial differential equations (PDEs) represented a 3D nanofluid bio convection model near a stagnation point. The model expresses the conservation of momentum, microorganisms, thermal energy, nanoparticles and total mass via a set of governing equations. We use Buongiorno's setting to obtain a generated system and reduce it to nonlinear ordinary differential equations (NODEs). This initial system of PDEs that transferred to NODEs is solved based on the collocation discretization and tackled through the Euler wavelet truncated representation generated by a set of functions Involving matrix inversion. The scheme presents a meaningful and accurate numerical solution based on the numerical evidences and graphical illustration for several parameters. This confirms the efficiency of the proposed method and can be extended to other types of NODEs.

Introduction

In the new era of fluids, free-convection flows in 3D at the point where the fluid flow field presented at rest on the surface of objects (the stagnation point) have accomplished a substantial devotion. This is due to their capability and valuable applications in industry, manufacturing processes, and many more. Among these, the solutions of the boundary layer flows near a 3D stagnation point on an isothermal surface have been explored in many settings, see for example [1,2]. Poots in [3] analyzed based on three factors the flow of a saddle point of accessory. A great contribution on the hybrid nanofluid can be seen in [4]. Some other related bio-convection studies can be found in [5–8]. It is important here to mention the significant development in bio-convection has been achieved by the researchers in [9–12].

In this work, we apply the wavelet truncated expansion generated by a specific construction in the numerical solution of the reduced NODEs. Wavelets have the right structure to capture the sparsity in linear and non-linear systems under the current setting, its normality, and the right approximating structure based on the proposed construction are the key role for the numerical solution of the general NODEs in this framework. Recently, some authors have been considering an effective approaches to solve systems of differential equations such as those in [13–16]. Here, to solve the proposed NODEs we use Euler wavelets expansion generated via Euler polynomials and based on collocation technique that was presented in [17].

We start with the mathematical model presented in [18,19]. Note that, the steady, viscous and incompressible convection nanofluid flow is considered in the mathematical formulation for the model. Assume that the flow covers nano-size particles in addition to the motile microorganisms in the region of the three dimensional stagnation point, taking into account that the object surface is in the x and y coordinates, and z-axis is orthogonal to the surface of the object. Given that, the temperature P_w, density of motile microorganisms D_w and the volume fraction V_w have the constant values of P_∞; D_∞ and V_∞, we have the following system of nonlinear PDEs as in [18,19] such that

$$\begin{aligned}
u_x + v_y + w_z &= 0,\\
\rho_g\left(uu_x + vu_y + wu_z\right) - \mu\left(uu_{xx} + vu_{yy} + wu_{zz}\right) &= ax\left(\rho_g\beta(1-V_w)(P-P_\infty) - \gamma\Delta\rho(\rho-\rho_g)(V-V_\infty)\right)\\
\rho_g\left(uv_x + vv_y + wv_z\right) - \mu\left(uv_{xx} + vv_{yy} + wv_{zz}\right) &= by\left(\rho_g\beta(1-V_w)(P-P_\infty) - \gamma\Delta\rho(\rho-\rho_g)(V-V_\infty)\right)\\
uP_x + vP_y + wP_z - \alpha(P_{xx} + P_{yy} + P_{zz}) &= \tau D_\infty\left(P_xV_x + P_yV_y + P_zV_z + P_x^2 + P_y^2 + P_z^2\right)\\
uV_x + vV_y + wV_z - D_\infty(V_{xx} + V_{yy} + V_{zz}) &= \tau D_\infty/c\left(V_x^2 + V_y^2 + V_z^2\right)\\
uD_x + vD_y + wD_z + (O\overline{v_x})_x + (O\overline{v_y})_y + (O\overline{v_z})_z &= D_\infty(D_{xx} + D_{yy} + D_{zz}),
\end{aligned}$$

* Corresponding author.
E-mail addresses: Mutaz.Mohammad@zu.ac.ae (M. Mohammad), trounev.a@edu.kubsau.ru (A. Trounev), Mohammed.Alshbool@zu.ac.ae (M. Alshbool), line1@wit.edu (E.-B. Lin).

https://doi.org/10.1016/j.rinp.2022.105889
Received 22 June 2022; Received in revised form 28 July 2022; Accepted 10 August 2022
Available online 24 August 2022

where $\overline{v} = ObW\nabla c$. The boundary conditions BCs of the above setting is given by

$$P = P_w, D = D_w, V = V_w, u = 0, v = 0, w = 0 \quad when \quad z \to 0$$
$$P = P_\infty, D = D_\infty, V =_\infty, u = 0, v = 0 \quad when \quad z \to \infty$$

Now, under the similarity condition given in [18],

$$\begin{aligned} u &= vr^{0.5}xg'(\eta)a^2G, \\ v &= vr^{0.5}ys'(\eta)a^2G, \\ w &= -vr^{0.5}x(cs(\eta)+g(\eta)), \\ \theta(\eta) &= P - P_\infty/\left(P_w - P_\infty\right), \\ \phi(\eta) &= V - V_\infty/\left(V_w - V_\infty\right), \\ (\eta) &= D - D_\infty/\left(D_w - D_\infty\right), \\ \eta &= ae^{0.25}zG, \end{aligned}$$

and the following components transformation,

$$x, y \to \Big(ax\beta\rho_\infty(1-V_w)(P-P_\infty) - ax(\rho_g - \rho_{g_\infty})(V-V_\infty) + \gamma ax(D-D_\infty)\Big), z \to 0,$$

the above system of nonlinear PDEs can be transferred into the following set of NODEs where

$$g''(\eta)(cs(\eta)+g(\eta)) + g^{(3)}(\eta) - g'(\eta)^2 - \frac{\mathrm{Nr}\phi(\eta)}{\mathrm{Gr}\,\mathrm{Pr}} + \frac{\mathrm{Rab}\xi(\eta)}{\mathrm{Gr}} + \theta(\eta) = 0 \quad (1)$$

$$s^{(3)}(\eta) + (g(\eta)+cs(\eta))s''(\eta) - cs'(\eta)^2 + \theta(\eta) - Nr/(PrGr)\phi(\eta) + Rab/Gr(\xi)(\eta) = 0 \quad (2)$$

$$\mathrm{Pr}\,\theta'(\eta)(cs(\eta)+g(\eta)) + \mathrm{NB}\theta'(\eta)\phi'(\eta) + \mathrm{NT}\theta'(\eta)^2 + \theta''(\eta) = 0 \quad (3)$$

$$\mathrm{Le}\,\mathrm{Pr}\,\phi'(\eta)(cs(\eta)+g(\eta)) + \frac{\mathrm{NT}\theta''(\eta)}{\mathrm{NB}} + \phi''(\eta) = 0 \quad (4)$$

$$\mathrm{Sc}\xi'(\eta)(cs(\eta)+g(\eta)) - \mathrm{Pe}\left(\xi'(\eta)\phi'(\eta) + \xi(\eta)\phi''(\eta)\right) + \xi''(\eta) = 0, \quad (5)$$

with the BCs given by

$$g(0) = 0, f'(0) = 0, s(0) = 0, s'(0) = 0, \theta(0) = 1, \phi(0) = 1, \quad (6)$$

$$\xi(0) = 1, g'(L) = 0, s'(L) = 0, \theta(L) = 0, \phi(L) = 0, \xi(L) = 0, \quad (7)$$

where

$$Gr = \rho_{g_\infty}(P_w - P\infty)(1-V_\infty)/(v^2a^3\rho_g), Nr = g(V_w - V_\infty)(\rho - \rho_\infty)/(a^3\mu),$$

$$Pr = v/\alpha, Le = \alpha/D_w, Nt = \tau(P_w - P\infty)/\alpha, N_B = \tau(V_w - V\infty)/\alpha.$$

The numerical solution via Euler wavelets

The Euler polynomial $E_j(x), j = 1, 2, \ldots$, can be calculated by the below equation such that

$$\sum_{j\in\mathbb{Z}^+}^{\infty} \frac{E_k(x)t^k}{k!} = e^{xt}\left(e^t+1\right)^{-1},$$

where $E_0 = 1$. The first few polynomials are given explicitly as

$$\begin{aligned} E_1(x) &= x - 0.5, \\ E_2(x) &= x^2 - x, \\ E_3(x) &= x^3 - \frac{3x^2}{2} + 0.25, \\ E_4(x) &= x^4 - 2x^3 + x, \\ E_5(x) &= x^5 - \frac{5x^4}{2} + \frac{5x^2}{2} - 0.5, \\ E_6(x) &= x^6 - 3x^5 + 5x^3 - 3x, \\ E_7(x) &= x^7 - \frac{7x^6}{2} + \frac{35x^4}{4} - \frac{21x^2}{2} + \frac{17}{8}. \end{aligned}$$

Now we define the needed functions to illustrate the numerical technique as follows:

$$E_1(x) = -0.5 + x, \quad E_2(x) = -x + x^2, \quad (8)$$

$$I_1^1 = \int_0^x E_1(t)dt \quad (9)$$

$$I_2^1 = \int_0^x E_2(t)dt \quad (10)$$

$$I_1^2 = \int_0^x I_1^1(t)dt \quad (11)$$

$$I_2^2 = \int_0^x I_2^1(t)dt. \quad (12)$$

Define Ξ to be the set of all functions given in Eqs. (8)–(12). For any function $\tau \in \Xi$, we define the function $\varphi(x)$ as

$$\varphi(t) = \tau\chi_{[0,1]}(t),$$

where $\chi_{[0,1]}$ is the indicator function on [0,1]. Assume that

$$\varphi_1 = E_1, \varphi_2 = E_2, \varphi_{1,1} = I_1^1, \varphi_{2,1} = I_2^1, \varphi_{1,2} = I_1^2, \varphi_{2,2} = I_2^2,$$

we define the following set of wavelets, where $j, k \in \mathbb{Z}$ as

$$\begin{aligned} \varphi_1(j,k,t) &= \varphi_1(2^jt - k), \\ \varphi_2(j,k,t) &= \varphi_2(2^jt - k), \\ \varphi(j,k,t) &= (\varphi_1(j,k,t) + \varphi_2(j,k,t)), \\ \varphi^{1,1}(j,k,t) &= \varphi_{1,1}(2^jt - k), \\ \varphi^{1,2}(j,k,t) &= \varphi_{1,2}(2^jt - k), \\ \varphi^{2,1}(j,k,t) &= \varphi_{2,1}(2^jt - k), \\ \varphi^{2,2}(j,k,t) &= \varphi_{2,2}(2^jt - k), \\ \varphi^1(j,k,t) &= (\varphi^{1,1}(j,k,t) + \varphi^{2,1}(j,k,t))/j, \\ \varphi^2(j,k,t) &= (\varphi^{2,1}(j,k,t) + \varphi^{2,2}(j,k,t))/j^2. \end{aligned}$$

Recall that, see e.g. [17], a function $\tau \in L_2(\mathbb{R})$ can be expanded using the following series,

$$\tau(\eta) = \sum_{\ell=1}^{2}\sum_{j,k\in\mathbb{Z}}^{\infty} d_{j,k}^{\ell}\varphi_{j,k}^{\ell}(\eta), \quad (13)$$

where,

$$d_{j,k}^{\ell} = \left\langle \tau, \varphi_{j,k}^{\ell}(\eta)\right\rangle = \int_{\mathbb{R}} \tau(\eta)\varphi_{j,k}^{\ell}(\eta)w(x)d\eta,$$

in which $\langle\cdot,\cdot\rangle$ denotes the usual inner product over the space $L_2(\mathbb{R})$ and w is a proper weight function.

One may truncate Eq. (13) by $\tau_{n,M}$ where

$$\tau_{n,M}(t) = \sum_{\ell=1}^{2}\sum_{j=0}^{n}\sum_{k=0}^{M-1} d_{j,k}^{\ell}\varphi_{j,k}^{\ell}(t). \quad (14)$$

Therefore,

$$\|\tau - \tau_{n,M}\|_2^2 = \left\|\sum_{\ell=1}^{2}\sum_{j\geq n+1}\sum_{k\geq M+1} d_{j,k}^{\ell}\varphi_{j,k}^{\ell}(t)\right\|_2^2$$

To solve the proposed NODEs (1)-(7), we construct a vector Ξ_τ of length $M = 2^{n+1}, n \in \mathbb{N}$, such that

$$\Xi_\tau = [\varphi_\tau, \sigma^\kappa(1,0,x), \ldots, \sigma^\kappa(2^j,k,x), \ldots, \sigma^\kappa(2^n, 2^{n-1}, x)],$$
$$j = 0, 1, 2, \ldots, n; k = 0, 1, 2, \ldots, 2^{j-1},$$

where,

$$\begin{cases} \varphi_\tau = 1, \sigma^\kappa = \varphi & when\ \tau = E_1, E_2, \quad \kappa = 1, \\ \varphi_\tau = x, \sigma^\kappa = \varphi^1 & when\ \tau = I_1^1, I_2^1, \quad \kappa = j, \\ \varphi_\tau = x^2/2, \sigma^\kappa = \varphi^2 & when\ \tau = I_1^2, I_2^2, \quad \kappa = j^2. \end{cases}$$

As an illustration, when $n = 2$, we have:

- When $\varphi_\tau = 1, \kappa = 1$, we have

$$\Xi_\tau = \begin{cases} [1, 0, \ldots, 0] & x \in \mathbb{R} - [0, 1) \\ \left[1, x^2 - 0.5, 0, 4x^2 - 4x + 0.5, 0, 0, 0, 16x^2 - 24x + 8.5\right] & x \in [0.75, 1) \\ \left[1, x^2 - 0.5, 0, x^2 - 4x + 0.5, 0, 0, 16x^2 - 16x + 3.5, 0\right] & x \in [0.5, 0.75) \\ \left[1, x^2 - 0.5, 4x^2 - 0.5, 0, 0, 0.5 - 8x + 16x^2, 0, 0\right] & x \in [0.25, 0.5) \\ \left[1, x^2 - 0.5, 4x^2 - 0.5, 0, 16x^2 - 0.5, 0, 0, 0\right] & \text{True} \end{cases}$$

- When $\varphi_\tau = x, \kappa = j$,

$$\Xi_\tau = \begin{cases} [x, 0, \ldots, 0] & x \in \mathbb{R} - [0, 1) \\ [x, \frac{x^3}{3} - \frac{x}{2}, 0, \frac{4x^3}{3} - 2x^2 + \frac{x}{2} \\ + \frac{1}{12}, 0, 0, 0, \frac{16x^3}{3} - 12x^2 + \frac{17x}{2} - \frac{15}{8}] & x \in [0.75, 1) \\ [x, \frac{x^3}{3} - \frac{x}{2}, 0, \frac{4x^3}{3} - 2x^2 + \frac{x}{2} + 0.0833333, 0, 0, \\ \frac{16x^3}{3} - 8x^2 + \frac{7x}{2} - \frac{5}{12}, 0] & x \in [0.5, 0.75) \\ [x, \frac{x^3}{3} - \frac{x}{2}, \frac{4x^3}{3} - \frac{x}{2}, 0, 0, \frac{16x^3}{3} - 4x^2 + \frac{x}{2} + \frac{1}{24}, 0, 0] & x \in [0.25, 0.5) \\ [x, \frac{x^3}{3} - \frac{x}{2}, \frac{4x^3}{3} - \frac{x}{2}, 0, \frac{16x^3}{3} - \frac{x}{2}, 0, 0, 0] & \text{True} \end{cases}$$

- When $\varphi_\tau = x^2/2, \kappa = j^2$, we have

$$\Xi_\tau = \begin{cases} [0.5x^2, 0, \ldots, 0] & x \in \mathbb{R} - [0, 1) \\ [0.5x^2, \frac{x^4}{12} - \frac{x^2}{4}, 0, \frac{x^4}{3} - \frac{2x^3}{3} + \frac{x^2}{4} + \frac{x}{12} \\ - \frac{1}{24}, 0, 0, 0, \frac{4x^4}{3} - 4x^3 + \frac{17x^2}{4} - \frac{15x}{8} + \frac{9}{32}] & x \in [0.75, 1) \\ [0.5x^2, \frac{x^4}{12} - \frac{x^2}{4}, 0, \frac{x^4}{3} - \frac{2x^3}{3} + \frac{x^2}{4} + \frac{x}{12} \\ - \frac{1}{24}, 0, 0, \frac{4x^4}{3} - \frac{8x^3}{3} + \frac{7x^2}{4} - \frac{5x}{12} + \frac{1}{48}, 0] & x \in [0.5, 0.75) \\ [0.5x^2, \frac{x^4}{12} - \frac{x^2}{4}, \frac{x^4}{3} - \frac{x^2}{4}, 0, 0, 48x^4 - 28x^3 \\ - \frac{47x^2}{12} + \frac{11x}{24} - \frac{1}{96}, 0, 0] & x \in [0.25, 0.5) \\ [0.5x^2, \frac{x^4}{12} - \frac{x^2}{4}, \frac{x^4}{3} - \frac{x^2}{4}, 0, \frac{4x^4}{3} - \frac{x^2}{4}, 0, 0, 0] & \text{True} \end{cases}$$

The mathematical procedure

Now, we define the approximate solution of Eqs. (1)–(5) based on the truncated Euler expansion defined in Eq. (14) as follows

$$g^{(3)}(\eta) \approx \widetilde{g}(\eta) = \sum_{\ell=1}^{2}\sum_{j=0}^{n}\sum_{k=0}^{M-1} d_{j,k}^{\ell,g}\varphi^{\ell}(\eta), \tag{15}$$

$$s^{(3)}(\eta) \approx \widetilde{s}(\eta) = \sum_{\ell=1}^{2}\sum_{j=0}^{n}\sum_{k=0}^{M-1} d_{j,k}^{\ell,s}\varphi^{\ell}(\eta), \tag{16}$$

$$\theta''(\eta) \approx \widetilde{\theta}(\eta) = \sum_{\ell=1}^{2}\sum_{j=0}^{n}\sum_{k=0}^{M-1} d_{j,k}^{\ell,\theta}\varphi^{\ell}(\eta), \tag{17}$$

$$\xi''(\eta) \approx \widetilde{\xi}(\eta) = \sum_{\ell=1}^{2}\sum_{j=0}^{n}\sum_{k=0}^{M-1} d_{j,k}^{\ell,\xi}\varphi^{\ell}(\eta), \tag{18}$$

$$\phi''(\eta) \approx \widetilde{\phi}(\eta) = \sum_{\ell=1}^{2}\sum_{j=0}^{n}\sum_{k=0}^{M-1} d_{j,k}^{\ell,\phi}\varphi^{\ell}(\eta). \tag{19}$$

Hence,

$$g(\eta) \approx \iint_\eta \widetilde{g} = \sum_{\ell=1}^{2}\sum_{j=0}^{n}\sum_{k=0}^{M-1} d_{j,k}^{\ell,g}\iint_\eta \varphi_{j,k}^{\ell}, \tag{20}$$

$$s(\eta) \approx \iint_\eta \widetilde{s} = \sum_{\ell=1}^{2}\sum_{j=0}^{n}\sum_{k=0}^{M-1} d_{j,k}^{\ell,s}\iint_\eta \varphi_{j,k}^{\ell}, \tag{21}$$

$$\theta(\eta) \approx \iint_\eta \widetilde{\theta} = \sum_{\ell=1}^{2}\sum_{j=0}^{n}\sum_{k=0}^{M-1} d_{j,k}^{\ell,\theta}\iint_\eta \varphi_{j,k}^{\ell}, \tag{22}$$

$$\xi(\eta) \approx \iint_\eta \widetilde{\xi} = \sum_{\ell=1}^{2}\sum_{j=0}^{n}\sum_{k=0}^{M-1} d_{j,k}^{\ell,\xi}\iint_\eta \varphi_{j,k}^{\ell}, \tag{23}$$

$$\phi(\eta) \approx \iint_\eta \widetilde{\phi} = \sum_{\ell=1}^{2}\sum_{j=0}^{n}\sum_{k=0}^{M-1} d_{j,k}^{\ell,\phi}\iint_\eta \varphi_{j,k}^{\ell}. \tag{24}$$

Using Eqs. (16)–(20), the NODEs given by Eqs. (1)–(5) yields the following

$$\int_\eta \widetilde{g}(t)dt\left(c\iiint_\eta(\widetilde{s}(t)+\widetilde{g}(t))dt\right) - \left(\iint_\eta \widetilde{g}(t)dt\right)^2 - \frac{\mathrm{Nr}\iiint_\eta \widetilde{\phi}(t)dt}{\mathrm{Gr}\,\mathrm{Pr}} + \frac{\mathrm{Rab}\iiint_\eta \widetilde{\xi}(t)dt}{\mathrm{Gr}} + \iiint_\eta \widetilde{\theta}(t)dt = 0$$

$$\widetilde{s}(\eta) + \left(\iiint_\eta \widetilde{g}(t)dt + c\iiint_\eta \widetilde{s}(t)dt\right)\int_\eta \widetilde{s}(t)dt - c\left(\iint_\eta \widetilde{s}(t)dt\right)^2 + \iiint_\eta \widetilde{\theta}(t)dt - \frac{Nr}{PrGr}\iiint_\eta \widetilde{\phi}(t)dt + \frac{Rab}{Gr}\iiint_\eta \widetilde{\xi}(t)dt = 0$$

$$Pr\iint_\eta \widetilde{\theta}(t)dt\left(c\iiint_\eta \widetilde{s}(t)dt + \iiint_\eta \widetilde{g}(t)dt\right) + \mathrm{NB}\iiint_\eta \widetilde{\theta}(t)dt\int_\eta \widetilde{\phi}(t)dt + \mathrm{NT}\left(\iint_\eta \widetilde{\theta}(t)dt\right)^2 + \int_\eta \widetilde{\theta}(t)dt = 0$$

$$\mathrm{Le}\,\mathrm{Pr}\iint_\eta \widetilde{\phi}(t)dt\left(c\iiint_\eta \widetilde{s}(t)dt + \iiint_\eta \widetilde{g}(t)dt\right) + \frac{\mathrm{NT}\int_\eta \widetilde{\theta}(t)dt}{\mathrm{NB}} + \int_\eta \widetilde{\phi}(t)dt = 0$$

$$\mathrm{Sc}\iint_\eta \widetilde{\xi}(t)dt\left(c\iiint_\eta \widetilde{s}(t)dt + \iiint_\eta \widetilde{g}(t)dt\right) - \mathrm{Pe}\left(\iint_\eta \widetilde{\xi}(t)dt\iint_\eta \widetilde{\phi}(t)dt + \iiint_\eta \widetilde{\xi}(t)dt\int_\eta \widetilde{\phi}(t)dt\right) + \int_\eta \widetilde{\xi}(t)dt = 0,$$

To implement the collocation point, we define

$$M = 2^{1+n}, n = 1, 2, \ldots,$$

as a collocation node where

$$s_i = s_{i-1} + 1/M, i = 1, 2, \ldots, M; \eta_i = \frac{1}{2}(s_{i-1} + s_i), i = 1, 2, \ldots, M.$$

Now, by substituting the collocation points to the system of equations above, we have

$$\int_{\eta_i} \widetilde{g}(t)dt\left(c\iiint_{\eta_i}(\widetilde{s}(t)+\widetilde{g}(t))dt\right) - \left(\iint_{\eta_i} \widetilde{g}(t)dt\right)^2 - \frac{\mathrm{Nr}\iiint_{\eta_i} \widetilde{\phi}(t)dt}{\mathrm{Gr}\,\mathrm{Pr}} + \frac{\mathrm{Rab}\iiint_{\eta_i} \widetilde{\xi}(t)dt}{\mathrm{Gr}} + \iiint_{\eta_i} \widetilde{\theta}(t)dt = 0$$

$$\widetilde{s}(\eta_i) + \left(\iiint_{\eta_i} \widetilde{g}(t)dt + c\iiint_{\eta_i} \widetilde{s}(t)dt\right)\int_{\eta_i} \widetilde{s}(t)dt - c\left(\iint_{\eta_i} \widetilde{s}(t)dt\right)^2 + \iiint_{\eta_i} \widetilde{\theta}(t)dt - \frac{Nr}{PrGr}\iiint_{\eta_i} \widetilde{\phi}(t)dt + \frac{Rab}{Gr}\iiint_{\eta_i} \widetilde{\xi}(t)dt = 0$$

$$Pr\iint_{\eta_i} \widetilde{\theta}(t)dt\left(c\iiint_{\eta_i} \widetilde{s}(t)dt + \iiint_{\eta_i} \widetilde{g}(t)dt\right) + \mathrm{NB}\iiint_{\eta_i} \widetilde{\theta}(t)dt\iint_{\eta_i} \widetilde{\phi}(t)dt + \mathrm{NT}\left(\iint_{\eta_i} \widetilde{\theta}(t)dt\right)^2 + \int_{\eta_i} \widetilde{\theta}(t)dt = 0$$

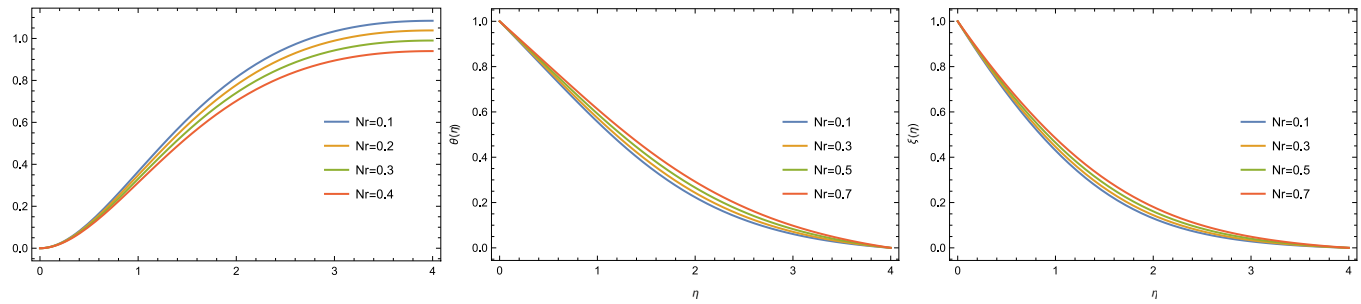

Fig. 1. The improvement of g, θ, and ξ verses Nr, receptively, when $c = 0, Pr = Gr = Pe = Le = Rab = Sc = 1, NB = NT = 0.1$.

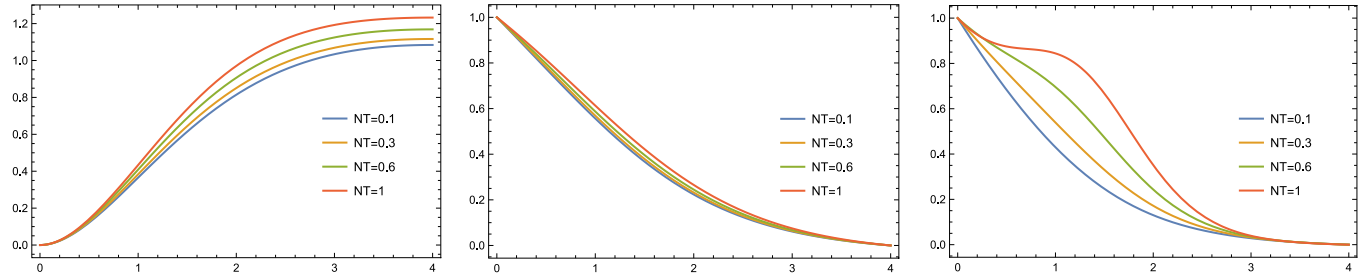

Fig. 2. The improvement of g, θ, and ξ verses NT, receptively, when $c = 0, Pr = Gr = Pe = Le = Rab = Sc = 1, NB = Nr = 0.1$.

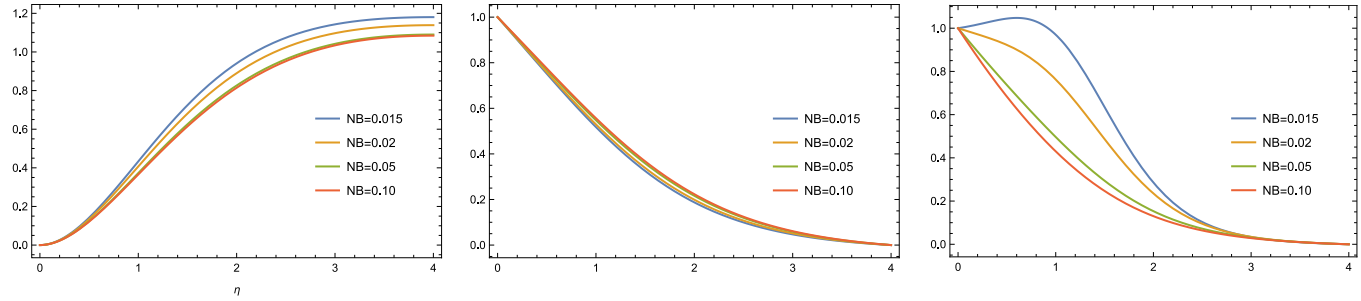

Fig. 3. The improvement of g, θ, and ξ verses NB, receptively, when $c = 0, Pr = Gr = Pe = Le = Rab = Sc = 1, Nr = NT = 0.1$.

$$\mathrm{Le\,Pr}\iint_{\eta_i}\widetilde{\phi}(t)dt\left(c\iiint_{\eta_i}\widetilde{s}(t)dt+\iiint_{\eta_i}\widetilde{g}(t)dt\right)+\frac{\mathrm{NT}\int_{\eta_i}\widetilde{\theta}(t)dt}{\mathrm{NB}}+\int_{\eta_i}\widetilde{\phi}(t)dt=0$$

$$\mathrm{Sc}\iint_{\eta_i}\widetilde{\xi}(t)dt\left(c\iiint_{\eta_i}\widetilde{s}(t)dt+\iiint_{\eta_i}\widetilde{g}(t)dt\right)-\mathrm{Pe}\left(\iint_{\eta_i}\widetilde{\xi}(t)dt\iint_{\eta_i}\widetilde{\phi}(t)dt+\iiint_{\eta_i}\widetilde{\xi}(t)dt\int_{\eta_i}\widetilde{\phi}(t)dt\right)+\int_{\eta_i}\widetilde{\xi}(t)dt=0,$$

Therefore, the collocation division generates a system of algebraic equations that can be solved easily by Mathematica software to produce the unknown coefficients $d^{\ell,g}_{j,k}, d^{\ell,s}_{j,k}, d^{\ell,\theta}_{j,k}, d^{\ell,\xi}_{j,k}$ and $d^{\ell,\phi}_{j,k}$ needed to find an approximate solutions given by Eqs. (16)–(20).

Graphical illustration

In this part, we present the behavior of the approximated functions g, θ, and ξ for some values of $c, P_r, G_r, P_e, L_e, R_{a_b}, S_c, N_B$, and N_T. More specifically, Figs. 1–9 illustrate the effect of g, θ, and ξ under $P_r, N_T, N_B, c, L_e, P_r, R_{a_b}$, and S_c, respectively. For example, with regards of ξ, we interpret the following:

- In a gradual way, the relation between the buoyancy ratio and ξ is clearly viewed in Fig. 1.
- The behavior of ξ is present when N_T increased as depicted in Fig. 2.
- The variation in ξ versus N_B is illustrated in Fig. 3. The effect of the ratio parameter on ξ profile is viewed in Fig. 4.
- The impact of Le on the density of xi is described in Fig. 5.
- The dual impact of Pr on ξ is depicted in Fig. 6.
- The behavior of ξ by increasing R_{a_b} exhibited in Fig. 7.
- The same behavior in ξ is gradually increased by the values of Sc, Pe respectively and displayed by Figs. 8, and 9.

Figs. 10–13 show the improvement in $g''(0)$, $-\theta''(0)$, $-\phi''(0)$ and $-\xi''(0)$ respectively by enhancing Nr, NB and, Nr, NT.

The graphical representation of square residual is depicted in Fig. 14, where it is clearly proves the reliability and accuracy of the used method along with the computational cost. In Table 1 we present the error bounds for each truncated parameter based on Euler wavelets by approximating the below integrals where

$$\Delta_g=\int_{\eta_\infty}\left(\widetilde{g}''(\eta)(c\widetilde{s}(\eta)+\widetilde{g}(\eta))+\widetilde{g}^{(3)}(\eta)-\widetilde{g}'(\eta)^2-\frac{\mathrm{Nr}\widetilde{\phi}(\eta)}{\mathrm{Gr\,Pr}}+\frac{\mathrm{Rab}\widetilde{\xi}(\eta)}{\mathrm{Gr}}+\widetilde{\theta}(\eta)\right)d\eta$$

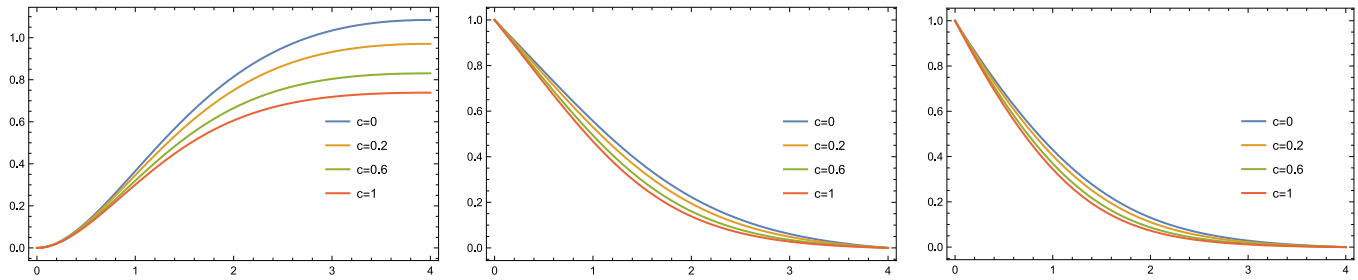

Fig. 4. The improvement of g, θ, and ξ verses c, receptively, when $Pr = Gr = Pe = Le = Rab = Sc = 1, Nr = NB = NT = 0.1$.

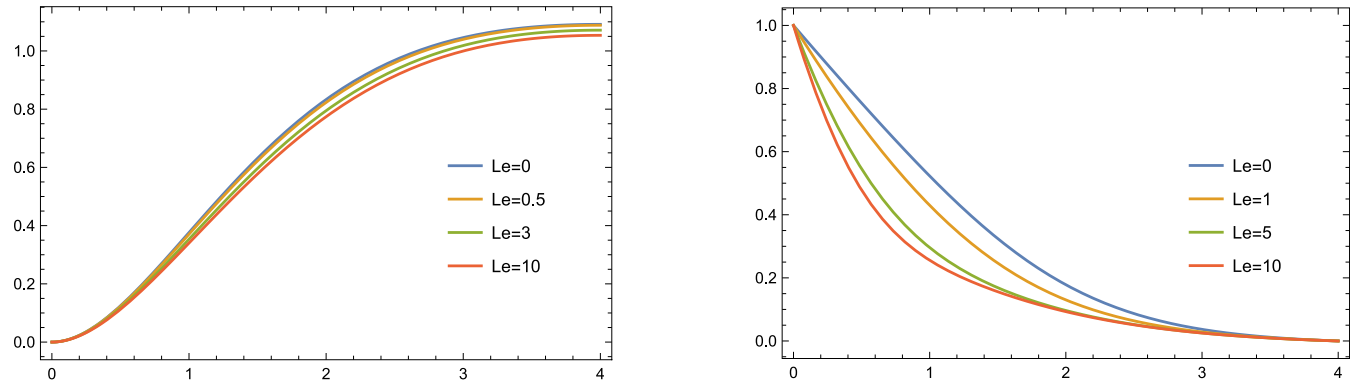

Fig. 5. The improvement of g, θ, and ξ verses Le, receptively, when $c = 0, Pr = Gr = Pe = Rab = Sc = 1, Nr = NB = NT = 0.1$.

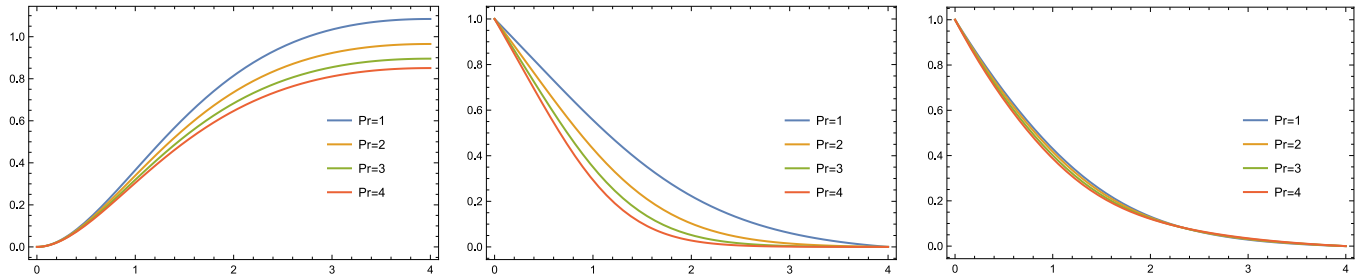

Fig. 6. The improvement of g, θ, and ξ verses Pr, receptively, when $c = 0, Le = Gr = Pe = Rab = Sc = 1, Nr = NB = NT = 0.1$.

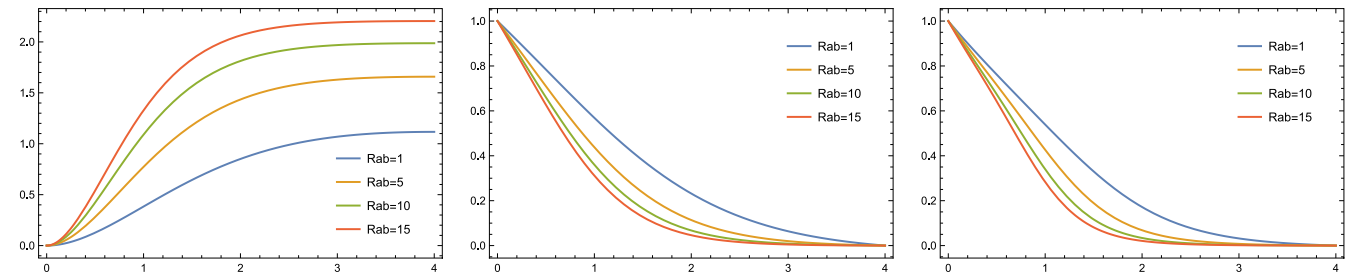

Fig. 7. The improvement of g, θ, and ξ verses R_{a_b}, receptively, when $c = 0, Le = Pr = Gr = Pe = Sc = 1, Nr = NB = 0.1, NT = 0.3$.

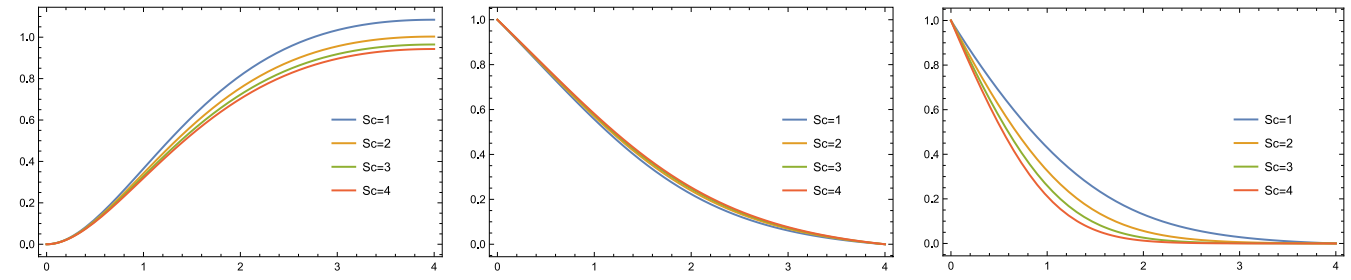

Fig. 8. The improvement of g, θ, and ξ verses S_c, receptively, when $c = 0, Le = Pr = Gr = Pe = Rab = 1, Nr = NB = NT = 0.1$.

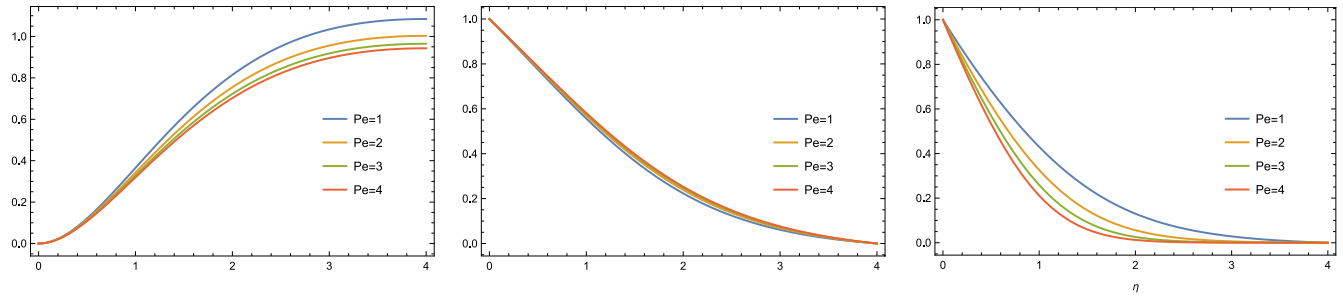

Fig. 9. The improvement of g, θ, and ξ verses Pe, receptively, when $c = 0, Le = Pr = Gr = Sc = Rab = 1, Nr = NB = NT = 0.1$.

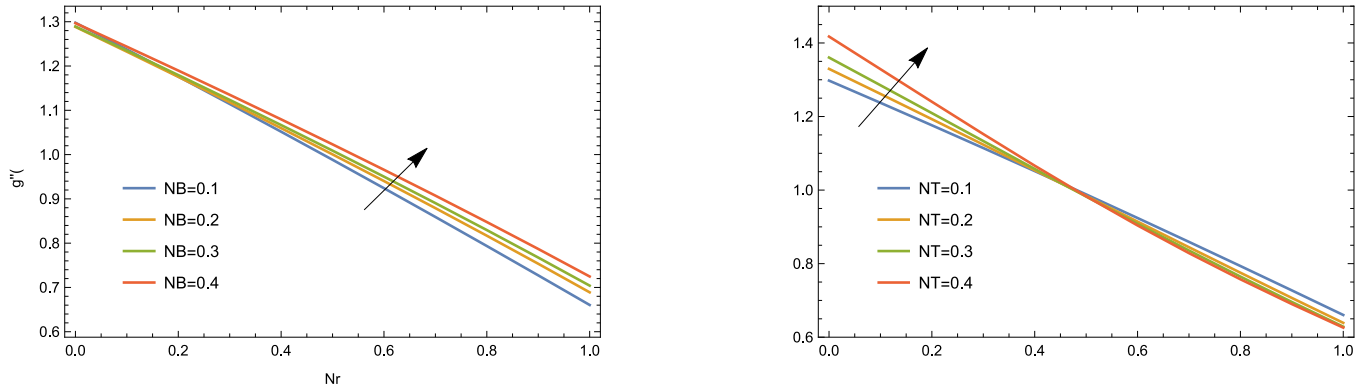

Fig. 10. The improvement of g'' verses Nr, NB and, Nr, N_T respectively when $Le = Pr = Gr = Sc = Rab = 1, c = NB = 0.1$.

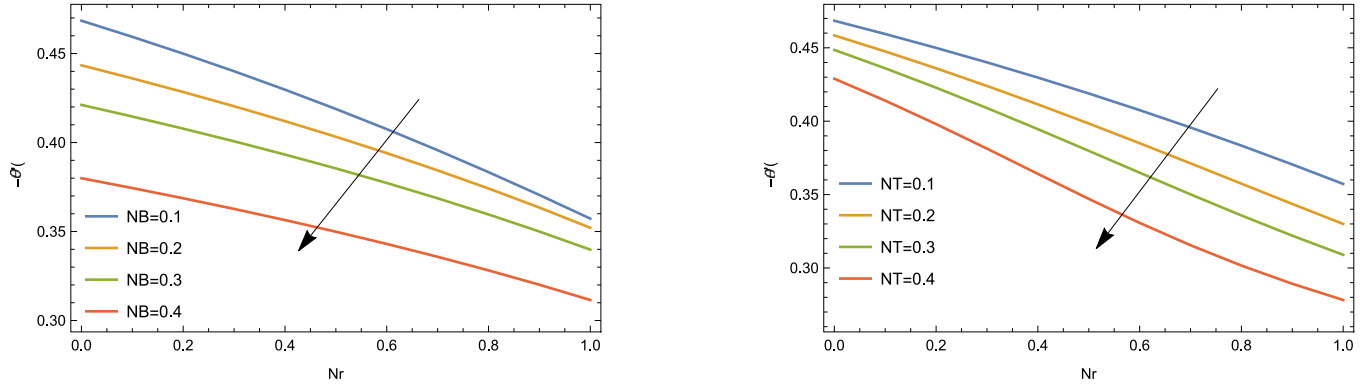

Fig. 11. The improvement of $-\theta'(0)$ verses Nr, NB and, Nr, N_T respectively when $Le = Pr = Gr = Sc = Rab = 1, c = NT = 0.1$.

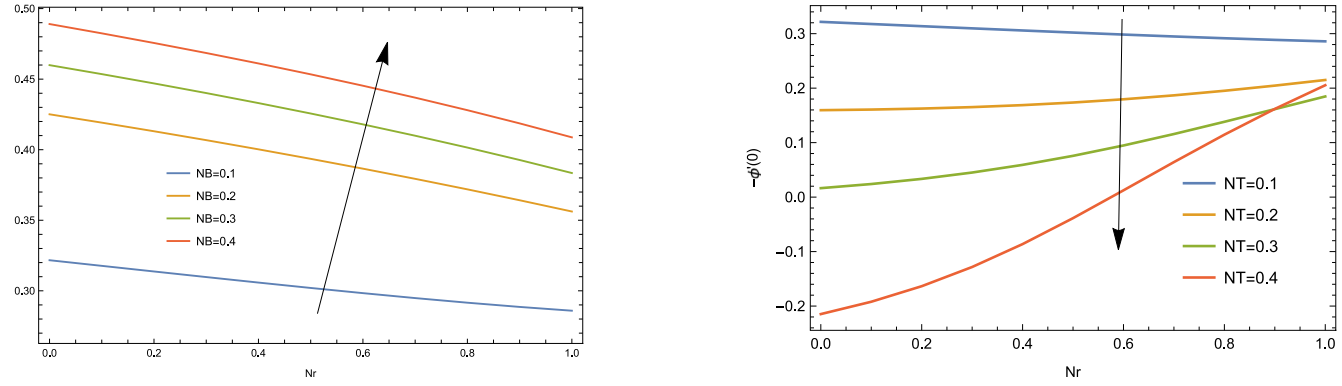

Fig. 12. The improvement of $-\phi'(0)$ verses Nr, NB and, Nr, N_T respectively when $Le = Pr = Gr = Sc = Rab = 1, c = NT = 0.1$.

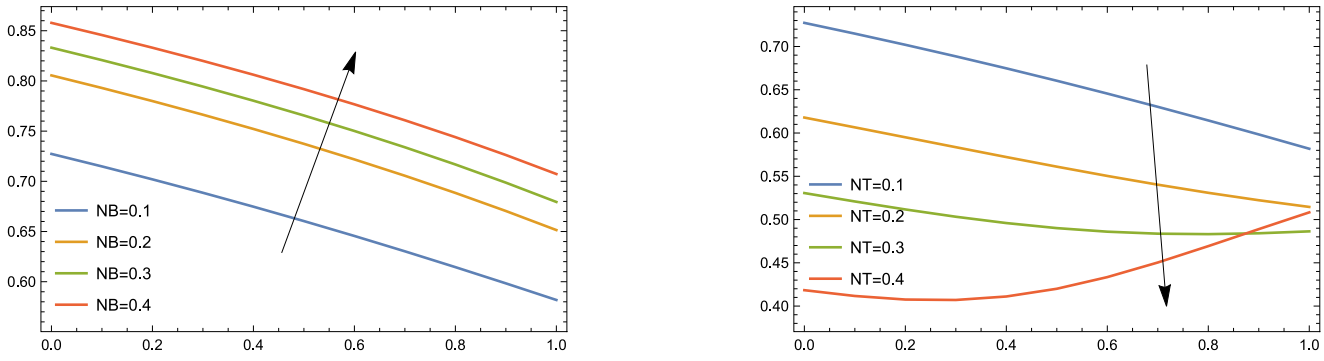

Fig. 13. The improvement of $-\xi'(0)$ verses Nr, NB and, Nr, N_T respectively when $Le = Pr = Gr = Sc = Rab = 1, c = NT = 0.1$.

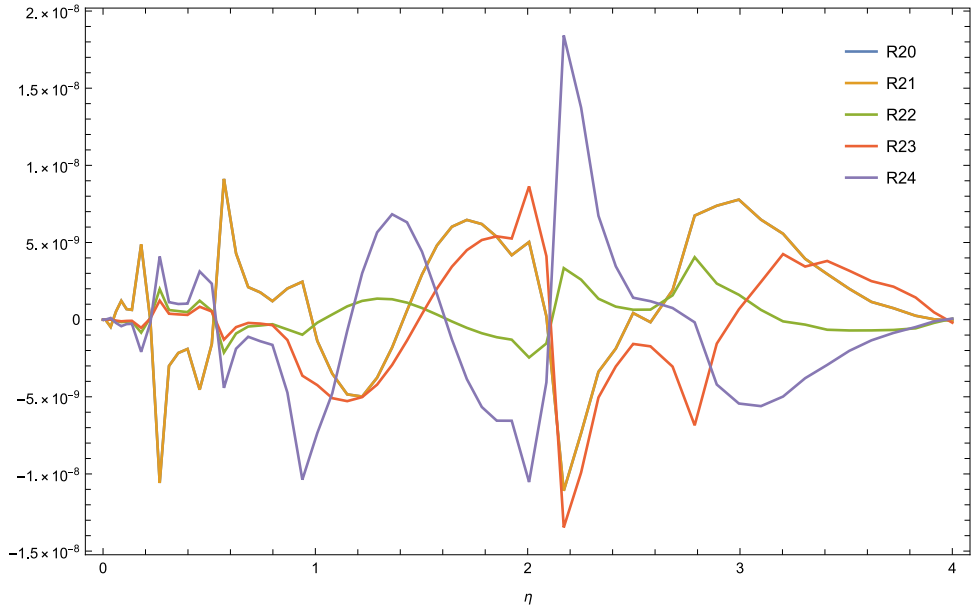

Fig. 14. The error bounds illustration.

Table 1
Some numerical evidences of square residual error versus approximations.

M	Δ_g	Δ_g	Δ_θ	Δ_ϕ	Δ_ξ	CPU time (s)
66	8.032×10^{-17}	8.032×10^{-17}	7.152×10^{-18}	6.629×10^{-17}	1.112×10^{-16}	32.639

$$\Delta_s = \int_{\eta_\infty} \left(\widetilde{s}^{(3)}(\eta) + (\widetilde{g}(\eta) + c\widetilde{s}(\eta))\widetilde{g}''(\eta) - c\widetilde{s}'(\eta)^2 + \widetilde{\theta}(\eta) - Nr/(PrGr)\widetilde{\phi}(\eta) + Rab/Gr(\widetilde{\xi})(\eta) \right) d\eta$$

$$\Delta_\theta = \int_{\eta_\infty} \left(\Pr \widetilde{\theta}'(\eta)(c\widetilde{s}(\eta) + \widetilde{g}(\eta)) + \mathrm{NB}\widetilde{\theta}'(\eta)\widetilde{\phi}'(\eta) + \mathrm{NT}\widetilde{\theta}'(\eta)^2 + \widetilde{\theta}''(\eta) \right) d\eta$$

$$\Delta_\phi = \int_{\eta_\infty} \left(\mathrm{Le}\Pr \widetilde{\phi}'(\eta)(c\widetilde{s}(\eta) + \widetilde{g}(\eta)) + \frac{\mathrm{NT}\theta''(\eta)}{\mathrm{NB}} + \widetilde{\phi}''(\eta) \right) d\eta$$

$$\Delta_\xi = \int_{\eta_\infty} \left(\mathrm{Sc}\widetilde{\xi}'(\eta)(c\widetilde{s}(\eta) + \widetilde{g}(\eta)) - \mathrm{Pe}\left(\widetilde{\xi}'(\eta)\widetilde{\phi}'(\eta) + \widetilde{\xi}(\eta)\widetilde{\phi}''(\eta) \right) + \widetilde{\xi}''(\eta) \right) d\eta.$$

Conclusion

The intended work is devoted to shedding some light on the use of wavelets through a new scheme in the area of numerical solutions of PDEs formed by various parameters in nanofluid applications. The Euler polynomials have been successfully applied to test the 3D nanofluid bio-convection model around a stagnation point. The generated system of PDEs has been reduced to a system of NODEs under the given governing equations. The solution of the reduced model is conducted by a new technique involved by a set of functions with proper translation and dilation.

This is a new contribution of using such wavelets in the area of nanofluids and we are certain that this contribution will open many doors for future investigations. Finally, it is remarkable to notice the error is decreased while M is increasing. This gives rise to the efficiency, accuracy and the low computational cost of the proposed method. We will explore our method in various PDEs in nanofluids.

Declaration of competing interest

The authors declare the following financial interests/personal relationships which may be considered as potential competing interests: Mutaz Mohammad reports article publishing charges was provided by Zayed University. Mutaz Mohammad reports a relationship with Zayed University that includes: employment.

Data availability

No data was used for the research described in the article.

References

[1] Howarth L. The boundary layer in the three-dimensional flow-part I I, the flow near the stagnation point. Phil Mag 1951;V42:1433–40.

[2] Davey A, Schofield D. Three dimensional flow near a two dimensional stagnation point. J Fluid Mech 1967;V28:149–51.

[3] Poots G. Laminar free convection near the lower stagnation point on an isothermal curved surface. Int J Heat Mass Transf 1964;7(8):863–74.

[4] Choi S. Enhancing thermal conductivity of fluids with nanoparticles. ASME Fluids Eng Div 1995.

[5] Pal D. Mixed convection-radiation on stagnation point flow of nanofluids over a stretching/shrinking sheet in a porous medium with heat generation and viscous dissipation. J Petrol Sci Eng 2015.

[6] Lok YY. Mixed convection flow near the axisymmetric stagnation point on a stretching or shrinking cylinder. Int J Therm Sci 2012.

[7] Mukhopadhyay S. Effect of thermal radiation on unsteady mixed convection flow and heat transfer over a porous stretching surface in porous medium. Int J Heat Mass Transfer 2009.

[8] Jamaludin A, Nazarb R, Pop I. Mixed convection stagnation-point flow of Cross fluid over a shrinking sheet with suction and thermal radiation. Physica A 2022;V585. http://dx.doi.org/10.1016/j.physa.2021.126398.

[9] Kuznetsov A, Avramenko A. Effect of small particles on the stability of bioconvection in a suspension of gyrotactic microorganisms in a layer of finite depth. Int Commun Heat Mass Transfer 2004;31(1):1–10. http://dx.doi.org/10.1016/S0735-1933(03)00196-9.

[10] Geng P, Kuznetsov A. Effect of small solid particles on the development of bioconvection plumes. Int Commun Heat Mass Transfer 2004;31(5):629–38. http://dx.doi.org/10.1016/S0735-1933(04)00050-8.

[11] Geng P, Kuznetsov A. Settling of bidispersed small solid particles in a dilute suspension containing gyrotactic micro-or- ganisms. Internat J Engrg Sci 2005;43(11–12):992–1010. http://dx.doi.org/10.1016/j.ijengsci.2005.03.002.

[12] Geng P, Kuznetsov A. Introducing the concept of effective diffusivity to evaluate the effect of bio-convection on small solid particles. Internat J Numer Methods Heat Fluid Flow 2005;7(2):321–38. http://dx.doi.org/10.1108/09615530510590597.

[13] Kumar A, Prakash A, Baskonus HM. The epidemic COVID-19 model via caputo–fabrizio fractional operator. Waves in Random and Complex Media; 2022, http://dx.doi.org/10.1080/17455030.2022.2075954.

[14] Dubey RS, Goswami P, Baskonus HM, Gomati T. On the existence and uniqueness analysis of fractional blood glucose-insulin minimal model. Int Jo Model, Simul, Sci Comput 2022. http://dx.doi.org/10.1142/S1793962323500083.

[15] Gao W, Baskonus HM. Deeper investigation of modified epidemiological computer virus model containing the Caputo operator. Chaos Solitons Fractals 2022;158(112050):1–6.

[16] Veeresha, Malagi NS, Prakasha DG, Baskonus HM. An efficient technique to analyze the fractional model of vector-Borne diseases. Phys Scr 2022;97(054004):1–19.

[17] Mohammad M, Trounev A, Alshbool M. A novel numerical method for solving fractional diffusion-wave and nonlinear fredholm and Volterra integral equations with zero absolute error. Axioms 2021;10(3):165. http://dx.doi.org/10.3390/axioms10030165.

[18] Zhao Q, Xu H, Tao L, Raees A, Sun Q. Three-dimensional free bio-convection of nanofluid near stagnation point on general curved isothermal surface. Appl Math Mech 2016;37(4):417.

[19] Buongiorno J. Convective transport in nanofluids. J Heat Transfer 2006;128(3):240–50.